Observation of Surface Dirac Cone in High-Quality Ultrathin Epitaxial Bi_2Se_3 Topological Insulator on AlN(0001) Dielectric

Polychronis Tsipas,[†] Evangelia Xenogiannopoulou,[†] Spyridon Kassavetis,[†] Dimitra Tsoutsou,[†] Evangelos Golias,[†] Calliope Bazioti,[‡] George P. Dimitrakopulos,[‡] Philomela Komninou,[‡] Hu Liang,[§] Matty Caymax,[§] and Athanasios Dimoulas[†,*]

[†]National Center for Scientific Research, DEMOKRITOS, 15310 Athens, Greece, [‡]Department of Physics, Aristotle University of Thessaloniki, GR-54124 Thessaloniki, Greece, and [§]Imec, Kapeldreef 75, Leuven, Belgium

ABSTRACT Bi_2Se_3 topological insulators (TIs) are grown on AlN(0001)/Si(111) substrates by molecular beam epitaxy. In a one-step growth at optimum temperature of 300 °C, Bi_2Se_3 bonds strongly with AlN without forming interfacial reaction layers. This produces high epitaxial quality Bi_2Se_3 single crystals with a perfect registry with the substrate and abrupt interfaces, allowing thickness scaling down to three quintuple layers (QL) without jeopardizing film quality. It is found by angle-resolved photoelectron spectroscopy that, remarkably, Bi_2Se_3 films maintain the 3D TI properties at very low thickness of 3QL (~2.88 nm), exhibiting top surface gapless metallic states in the form of a Dirac cone.

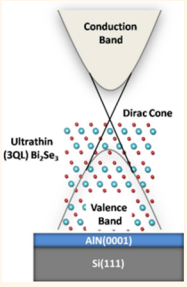

KEYWORDS: topological insulators · Bi_2Se_3 · ultrathin films · gapless surface metallic states · ARPES

Three-dimensional (3D) topological insulators (TIs) are materials that possess a bulk excitation gap and gapless surface metallic states, in the form of spin-polarized (helical) Dirac cones. TIs bring new physics in condensed matter[1,2] and show promise for spintronics devices and robust quantum computing. However, excess sensitivity of surface states under ambient conditions,[3,4] residual bulk conduction caused by defects,[5] and thermal excitations in the small bulk band gaps currently limit the study and utilization of the properties of the surface states for functional devices. Suppression of the bulk contribution can be obtained by improving their quality[6,7] and by growing TIs with relatively large band gaps, such as Bi_2Se_3 ($E_g \sim 0.3$ eV). On the other hand, ultrathin films offer the advantage of increased surface-to-volume ratio, enhancing surface state contribution, and making Bi_2Se_3 compatible with nanoelectronic device scaling trends. However, obtaining ultrathin epitaxial films with the properties of a 3D TI is not straightforward. Theoretical[8−12] and experimental[13−15] work indicates that below six quintuple layers (QLs), Bi_2Se_3 films show complex finite size effects,[8−12] manifested by energy gap opening[13−15] as a result of hybridization[8−11,13] of top and bottom surface bands. At lower thickness, a transition to nontrivial 2D quantum spin Hall (QSH) insulator[10,11,14] is predicted before the system falls into a trivial insulator state for thickness less than about 2QLs.[10,11] The presence of the substrate adds to the complexity because it can induce, in general, a surface inversion asymmetry[9] between the top and bottom surfaces of the TI, modifying the hybridization of the surface bands.[9,16−18] The substrate is an important factor from a technological perspective, too. It is highly preferable that TIs, Bi_2Se_3 in particular, are deposited on wide band gap (insulating) substrates to benefit from a Bi_2Se_3-on-insulator approach minimizing leakage currents through the substrate. While Bi_2Se_3 has been grown by molecular beam epitaxy (MBE) on several semiconductors (Si,GaAs, InP, CdS, In_2Se_3),[19−23] there is less work on epitaxial growth on crystalline dielectrics limited to sapphire substrates[6,15] and low gap $SrTiO_3$.[24]

Here we report on the epitaxial growth by MBE of very high quality Bi_2Se_3 on Al face AlN(0001)/Si(111) substrates prepared by

* Address correspondence to dimoulas@ims.demokritos.gr.

Received for review May 2, 2014 and accepted June 10, 2014.

Published online June 10, 2014
10.1021/nn502397x

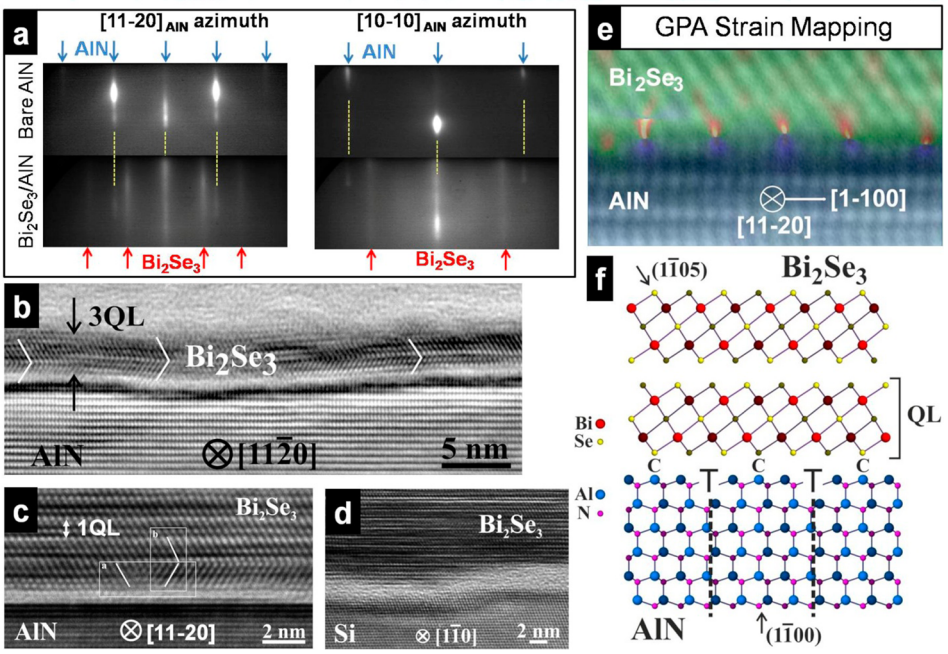

Figure 1. (a) RHEED patterns of 3QL Bi_2Se_3/AlN(0001) and bare AlN(0001) along [11−20] and [10−10] azimuths of AlN. (b,c) Cross-sectional HRTEM images of 3 and 5QL Bi_2Se_3, respectively, grown on AlN(0001) viewed along $[11-20]_{Bi_2Se_3}//[11-20]_{AlN}$. Rectangles a and b in (c) mark rotation (180°) and lamellar twins, respectively, which are observed in both samples. The interfaces are crystalline, albeit distorted. (d) HRTEM cross-sectional image of Bi_2Se_3 grown on Si(111) surface projected along $[11-20]_{Bi_2Se_3}//[1-10]_{Si}$, illustrating a distorted and partially crystalline interfacial region. All Bi_2Se_3 film depositions were performed at 300 °C. (e) Superimposed HRTEM with lattice strain map of the 3QL Bi_2Se_3/AlN(0001) sample showing the precise location of the misfit dislocations and the associated strain field components (tensile in red, compressive in blue) at the interface. (f) Schematic model of the matching between Bi_2Se_3 and AlN showing two mixed type misfit dislocations with extra half-planes on the substrate side. The projection direction is $[11-20]_{Bi_2Se_3}//[11-20]_{AlN}$. Two QLs are illustrated for Bi_2Se_3. The orientations of the $(1-100)_{AlN}$ and $(1-105)_{Bi2Se3}$ planes are indicated. Shading indicates distinct levels along the projection direction.

metal organic chemical vapor deposition. Films are prepared in a one-step growth process at an optimum temperature of 300 °C (see Experimental Section) and compared with Bi_2Se_3/Si control samples grown at the same temperature. Unlike sapphire, which is available only as bulk substrates, AlN can be grown epitaxially on large-area Si(111) wafers, holding promise for integration of Bi_2Se_3 with Si devices in a manufacturable Si-compatible process. More importantly, we report on the observation of gapless surface metallic states (Dirac cones) in ultrathin Bi_2Se_3 TIs down to 3QLs (<3 nm) thick and discuss the possible influence of the AlN substrate.

RESULTS AND DISCUSSION

Figure 1a shows the *in situ* reflection high-energy electron diffraction (RHEED) patterns of 3QL Bi_2Se_3/AlN(0001) structures and AlN(0001) substrate along [11−20] and [10−10] azimuths of AlN. Two distinct patterns corresponding to two different hexagonal lattices are observed with the inner streaks being attributed to Bi_2Se_3, while the outer ones are attributed to the AlN substrate, in agreement with a mismatch between the wurtzite AlN substrate ($\alpha_{AlN} \sim 3.11$ Å)[25] and rhombohedral Bi_2Se_3 ($\alpha_{Bi_2Se_3} \sim 4.14$ Å)[19,26] lattice constants. Despite the large lattice mismatch (~33%), RHEED indicates that the two hexagonal unit cells are perfectly aligned such that the $[11-20]_{Bi_2Se_3}//[11-20]_{AlN}$ is in-plane. It should be noted that we use four-axis hexagonal indexing for Bi_2Se_3, and this direction transforms to [110] in three-axis hexagonal notation. No signs of 30 or 90° rotational domains are observed in RHEED, indicating that Bi_2Se_3 is grown in single-crystal form. X-ray diffraction (XRD) (Supporting Information Figure S1) confirms the high crystalline quality of the films, providing evidence that the crystals are exclusively trigonal axis with the $[0001]_{Bi_2Se_3}//[0001]_{AlN}$ along the growth direction and that they have smooth and uniform surface and interfaces as can be inferred from pronounced Kiessig fringes (Figure S1).

The film microstructure is examined by high-resolution transmission electron microscopy (HRTEM) in cross-sectional geometry along the $[11-20]_{AlN}$ zone axis, and the images are presented in Figure 1b,c. The cross section of a Bi_2Se_3/Si(111) control sample is also presented in Figure 1d for comparison. Both 3 and 5QL Bi_2Se_3 in Figure 1b,c, respectively, indicate that $[11-20]_{Bi_2Se_3}//[11-20]_{AlN}$, thus confirming the in-plane epitaxial orientation relationship between the two materials previously deduced from RHEED (Figure 1a). Lamellar and 180° in-plane rotational domains are observed in the thicker but also the thinnest films

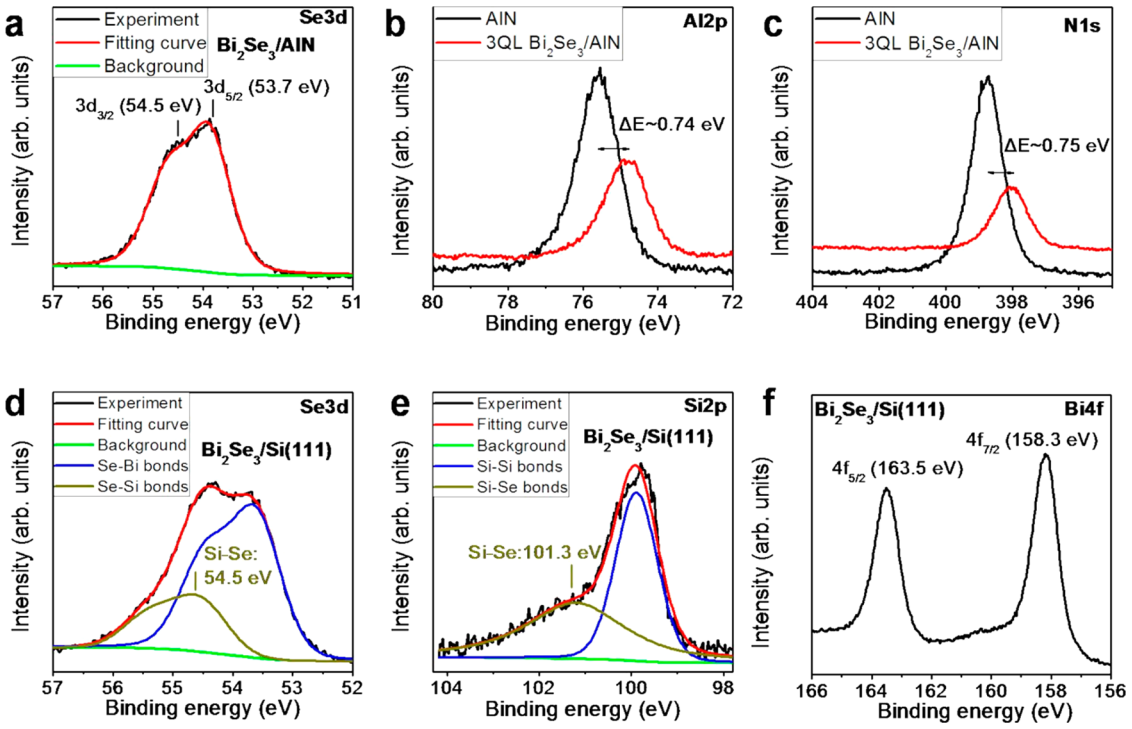

Figure 2. (a–c) Se 3d, Al 2p, and N 1s XPS spectra of a 3QL thick Bi_2Se_3 film deposited on AlN(0001) at 300 °C. No reaction with the substrate is observed, and the positions of the Se $3d_{5/2}$ and Se $3d_{3/2}$ peaks are in good agreement with those of bulk Bi_2Se_3 crystals. (d–f) Se 3d, Si 2p, and Bi 4f XPS spectra of a 3QL Bi_2Se_3 film deposited on Si(111) at 300 °C showing that Se reacts with Si at this temperature, forming Si–Se bonds.

(Figure 1b,c), similar to previous reports on Bi_2Se_3 grown on InP and Si[21] substrates. In Figure 1c, the different quintuple layers with a thickness of ~0.96 nm are clearly imaged, indicating that Bi_2Se_3 is grown such that $[0001]_{Bi_2Se_3}//[0001]_{AlN}$ is in agreement with XRD data (Figure S1). From Figure 1b,c, it can be inferred that Bi_2Se_3 forms with AlN crystalline abrupt interfaces (although distorted), as opposed to the case of Bi_2Se_3 control sample (Figure 1d) deposited at the same temperature of 300 °C where a thick interfacial layer is evident.

Strain mapping is performed using geometrical phase analysis (GPA)[27] in order to monitor the change of lattice constant and the atomic nanoscale localization of the misfit at the interface through misfit dislocations (MDs), as shown in Figure 1e. The MDs are introduced in order to accommodate the lattice mismatch, and in the present projection direction, they are manifested by considering the matching between the $(1\bar{1}00)_{AlN}$ planes that are vertical to the interface and the $(1\bar{1}05)_{Bi_2Se_3}$ that are inclined at 57.9°. Given that the spacing of the $(1\bar{1}00)_{AlN}$ planes is d_{AlN} = 2.69 Å, and the projected spacing of the $(1\bar{1}05)_{Bi_2Se_3}$ planes is ${}^{pr}d_{Bi_2Se_3} = d_{Bi_2Se_3}/\sin(57.9°) = 3.59$ Å, the misfit with respect to the AlN substrate is $f = ({}^{pr}d_{Bi_2Se_3}/d_{AlN}) - 1 = 33.2\%$, corresponding to 3:4 plane matching, consistent with the HRTEM observations (Figure 1e). Extra half-planes are localized at the substrate side as confirmed by the GPA analysis which clearly shows the tensile component of the MDs to be inside the epilayer (in red) and the compressive inside the AlN substrate (in blue). The corresponding crystallographic model is illustrated in Figure 1f.

The data in Figure 1 indicate that a coincidence lattice formed by exactly matching $3\alpha_{Bi_2Se_3}$ with $4\alpha_{AlN}$ (=12.44 Å) is the driving force for the perfect in-plane alignment of the two hexagonal lattices (Figure 1a) giving rise to a well-oriented single-crystalline epilayer. The formation of one MD every four substrate lattice planes (Figure 1e) facilitates lattice plane matching and promotes the high-quality epitaxial one-step growth at optimum temperature of 300 °C. This is to be contrasted with the case of Bi_2Se_3 on sapphire,[6] where, due to van der Waals epitaxy, Bi and Se interact very weakly with the substrate requiring a low-temperature/inferior quality buffer layer to achieve high-quality films in a two-step growth mode.

In Figure 2a–c, *in situ* X-ray photoelectron spectroscopy (XPS) data are presented for the 3QL Bi_2Se_3/AlN to study the possible reaction at the interface and compare with the 3QL Bi_2Se_3/Si control sample shown in Figure 2d–f. The line shapes of Bi (not shown here) and Se 3d peaks for the Bi_2Se_3/AlN sample are the same as the ones obtained in bulk Bi_2Se_3,[28] indicating that only Bi–Se bonds exist and that Bi_2Se_3 does not react with the AlN substrate, showing minimum interdiffusion, which is compatible with the rather sharp interfaces seen in HRTEM (Figure 1). The line shape of the Al 2p

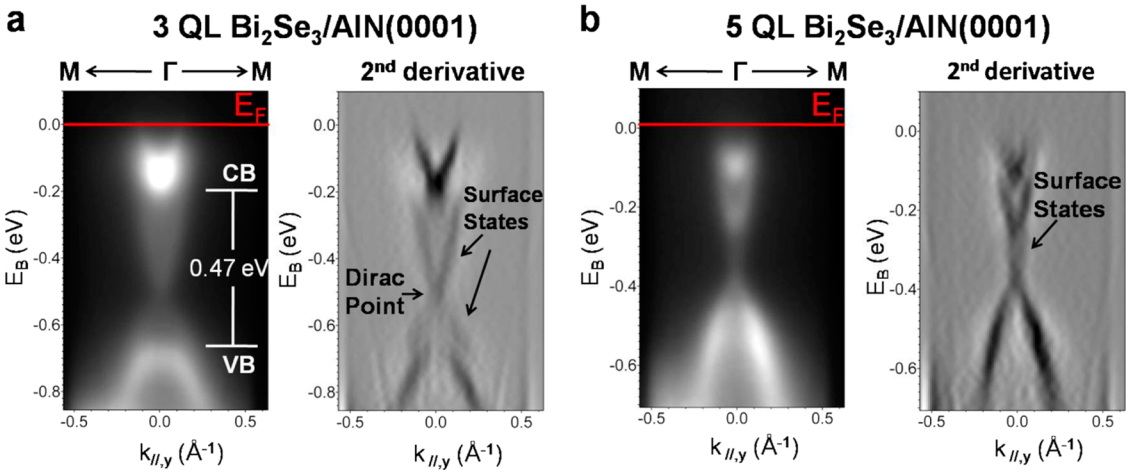

Figure 3. Band structure imaging by ARPES around the center (Γ) of the Brillouin zone of (a) 3QL and (b) 5QL thick Bi_2Se_3 films grown on AlN(0001) at 300 °C. The second derivative plot is also displayed. CB and VB denote the bulk-like conduction and valence bands, respectively. Gapless surface states in the form of Dirac cones are observed for both samples.

and N 1s peaks remains the same after growth of Bi_2Se_3, supporting the claim that there is no reaction at the interface. The ~0.75 eV shift to lower binding energies for both peaks after Bi_2Se_3 growth indicates a possible upward band bending of AlN near the interface to match the Fermi levels on both sides. On the other hand, the Se 3d and Si 2p peaks in Figure 2d,e, respectively, indicate that there is a strong reaction between Bi_2Se_3 and Si, in line with HRTEM observations (Figure 1d). Since the Bi 4f peaks in Figure 2f show no signs of Bi−Si bonds, it is concluded that the interfacial layer in Bi_2Se_3/Si control samples is due to Si−Se bonds only. In contrast to the case of Bi_2Se_3/Si where low temperature (<150 °C) buffer layers[29] are needed in order to avoid interfacial layers, Bi_2Se_3 can be grown with high epitaxial quality on AlN at an optimum temperature of 300 °C without the need for buffer layers, implying that, on AlN, the Bi_2Se_3 thickness can be aggressively scaled to less than 3QLs without jeopardizing structural quality and surface/interface integrity.

Figure 3 shows the band structure (a,c) of 3QL and 5QL thick Bi_2Se_3 deposited at 300 °C and their second derivatives along the M−Γ−M direction of the surface Brillouin zone imaged by *in situ* angle-resolved photoelectron spectroscopy (ARPES). For comparison, ARPES measurements on bulk Bi_2Se_3 crystals were also performed (Figure S2). Gapless surface states forming a Dirac cone are clearly seen in the second derivative spectrum, in addition to the bulk-like conduction and valence bands. The Dirac point (DP) is located at −0.5 eV from E_F, showing an n-type behavior possibly due to Se vacancies,[30] near the middle of the bulk-like band gap of ~0.47 eV. The latter is significantly higher than the 0.25 eV gap observed in the bulk Bi_2Se_3 control sample (Figure S2), showing the benefit of thickness reduction. To the best of our knowledge, the 3QL film in the present work is the thinnest Bi_2Se_3 where gapless surface states have ever been observed. It is worth noting that previous works on Bi_2Se_3 on double-layer graphene,[13] Si(111)$\beta\sqrt{3} \times \sqrt{3}$-Bi,[14] and α-$Al_2O_3$ (sapphire) substrates[15] report a gap opening when film thickness becomes less than 6QLs as a result of hybridization of Dirac cones at the top and bottom surfaces. Remarkably, our data are in reasonably good agreement with theoretical works[8,9,11] predicting an oscillatory behavior due to finite size effects. Indeed, our 3QL film thickness of ~2.88 nm is close to the predicted[10,12] critical thickness of 2.5 nm where the gap closes and reverses sign, marking the crossover[11] from a nontrivial 2D QSH to a trivial insulator state as thickness is reduced. Indirect evidence by ARPES of such a transition between 2 and 3QLs has already been reported, but a clear and sizable gap is observed in a 3QL film in that work.[14] The observation of gapless states in our 5QL film (Figure 3c,d) is in line with the theoretical predictions[8,9,11] of a negligibly small gap (~0.1 meV[8]) at around 5 nm (~5QLs) and only in rough qualitative agreement with the theoretical work in ref 10.

Since theoretical calculations[8−11] presume free-standing Bi_2Se_3 thin films, slight deviations between theory and experiment are expected because the influence of the substrate is not taken into account in these calculations. Indeed, the AlN may induce a high structural and physical/chemical asymmetry between the top and bottom interfaces. The dense 2D network of MDs and the associated localized strain at the bottom interface (Figure 1e) may alter the bottom surface states so that a strong hybridization is prevented, allowing for the observation of the top Dirac cone by ARPES (Figure 3a,b). In a similar way, the substrate could induce a strong band bending or potential gradient in the Bi_2Se_3 film, raising the energy position of the DP at the top surface relative to the bottom.[17] In fact, such a difference between top and bottom interface has been directly detected by low-temperature ARPES,[17] albeit in a thick 6QL film where hybridization

is less important. In our case of a thinner film (3QLs), a possible energy difference of the DPs could suppress hybridization near the DP, explaining our observations of gapless top surface bands. It should be noted that the polar nature[31] of the AlN substrate might also contribute to the asymmetry, thus amplifying the effect. Although the majority of the negative polarization charge induced by the Al face AlN will be balanced by the positive donor space charge at the depletion region near the n-type AlN top surface, a possible residual polarization charge could produce a sizable electric field at the interface with the Bi_2Se_3. In such a case, a large relative separation of the DPs between the top and bottom interfaces could be realized in line with predictions[16] of the effect of an interface electric field produced by a ferroelectric in contact with the TI.

CONCLUSION

In summary, it was proved that Bi_2Se_3 maintains the 3D TI properties at a layer thickness as small as 3QL, exhibiting a clear top surface gapless Dirac cone. The AlN(0001) substrate plays an important role because it allows a perfect registry of Bi_2Se_3 with the substrate surface and with minimum chemical reaction and interdiffusion at the interface. This promotes high-quality epitaxial growth at the optimum temperature of 300 °C in single-crystal form and with good interface integrity and allows one-step growth of Bi_2Se_3, without the need for a low-temperature buffer layer, offering excellent scaling of Bi_2Se_3 to a thickness as low as 3QL without jeopardizing film quality. Moreover, it is anticipated that the AlN substrate induces an asymmetry between the top and bottom interfaces, suppressing band hybridization that is an important requirement for the observation of gapless Dirac cones. Our ultrathin Bi_2Se_3 with gapless surface metallic states sitting on top of AlN insulator on silicon substrates presents an attractive structure for future TI devices that have a great potential for integration with conventional Si electronics.

EXPERIMENTAL SECTION

The experiments were carried out in an ultrahigh vacuum MBE system (base pressure in the 10^{-10} Torr range) equipped with RHEED and a UV and X-ray photoelectron spectrometer. The Bi_2Se_3 films were grown on Si(111)-7 × 7 and 200 nm AlN(0001)/Si(111) substrates under Se-rich conditions with a Se/Bi flux ratio of about 20. High-purity Bi (99.997%) and Se (99.999%) were both evaporated from Knudsen cells, while the growth rate was kept at 1.5QL/min. Films grown at temperatures less than 150 °C are of poor quality as indicated by RHEED diffused patterns. As the temperature increases up to 300 °C, the quality is substantially improved until the film becomes thermally unstable at much higher temperatures. Films of various thicknesses (3 to 23QLs) were grown at the optimum temperature of 300 °C. The 200 nm Al face AlN(0001) layers were epitaxially grown by MOCVD on B-doped p-type 200 mm Si(111) substrates, with a resistivity >1 Ω·cm. AlN is unintentionally n-type doped, typical for MOCVD-grown AlN layers. The AlN substrates received both *ex situ* and *in situ* cleaning in our MBE chamber.[32] First, they were immersed in acetone and methanol for 5 min in each solvent to decrease the surface C coverage. Subsequent dipping in a piranha solution (1:1 H_2O_2/H_2SO_4) reduced further the C contamination. A third wet cleaning step in HF solution (1:10 HF/H_2O) was followed to reduce the surface oxide. Subsequently, annealing in ultrahigh vacuum at 750 °C for 15 min was performed to obtain a clean surface free of C and negligible quantities of O contaminants as verified by *in situ* X-ray photoelectron spectroscopy. The Si(111) substrates were cleaned in vacuum by 1.5 keV Ar^+ ion sputtering for 10 min at 5×10^{-5} mbar. Subsequently, annealing in vacuum at 900 °C for 5 min was performed to cure Ar^+ ion sputtering damage and obtain the 7 × 7 reconstruction of silicon. The ARPES spectra were collected with a 100 mm hemispherical electron analyzer and a 2D charge-coupled device detector. The energy resolution of the detection system was better than 40 meV using a 21.22 eV photons from a He discharge source. The film nanostructure and thickness were determined by HRTEM. Cross-section TEM specimens were prepared by the sandwich technique. Mechanical grinding followed by focused Ar^+ ion milling in the GATAN PIPS was used to thin the specimens to electron transparency. HRTEM observations were performed using a 200 kV JEOL 2011 microscope. The film quality and structure were characterized by an *ex situ* X-ray diffraction system.

Conflict of Interest: The authors declare no competing financial interest.

Acknowledgment. This work is funded by the ERC Advanced Grant SMARTGATE-291260- "Smart Gates for the "Green" Transistor".

Supporting Information Available: Supplementary XRD spectrum of Bi_2Se_3 films and ARPES data of high-purity bulk Bi_2Se_3 crystals. This material is available free of charge *via* the Internet at http://pubs.acs.org.

REFERENCES AND NOTES

1. Hasan, M. Z.; Kane, C. L. Colloquium: Topological Insulators. *Rev. Mod. Phys.* **2010**, *82*, 3045–3067.
2. Qi, X.-L.; Zhang, S.-C. Topological Insulators and Superconductors. *Rev. Mod. Phys.* **2011**, *83*, 1057–1110.
3. Kong, D.; Cha, J. J.; Lai, K.; Peng, H.; Analytis, J. G.; Meister, S.; Chen, Y.; Zhang, H. J.; Fisher, I. R.; Shen, Z.-X.; *et al.* Rapid Surface Oxidation as a Source of Surface Degradation Factor for Bi_2Se_3. *ACS Nano* **2011**, *5*, 4698–4703.
4. Lang, M.; He, L.; Xiu, F.; Yu, X.; Tang, J.; Wang, Y.; Kou, X.; Jiang, W.; Fedorov, A. V.; Wang, K. L. Revelation of Topological Surface States in Bi_2Se_3 Thin Films by *In-Situ* Al Passivation. *ACS Nano* **2012**, *6*, 295–302.
5. Scanlon, D. O.; King, P. D. C.; Singh, R. P.; de la Torre, A.; McKeown Walker, S.; Balakrishnan, G.; Baumberger, F.; Catlow, C. R. A. Controlling Bulk Conductivity in Topological Insulators: Key Role of Anti-site Defects. *Adv. Mater.* **2012**, *24*, 2154–2158.
6. Taskin, A. A.; Sasaki, S.; Segawa, K.; Ando, Y. Achieving Surface Quantum Oscillations in Topological Insulator Thin Films of Bi_2Se_3. *Adv. Mater.* **2012**, *24*, 5581–5585.
7. Wang, G.; Zhu, X.-G.; Sun, Y.-Y.; Li, Y.-Y.; Zhang, T.; Wen, J.; Chen, X.; He, K.; Wang, L.-L.; Ma, X.-C.; *et al.* Topological Insulator Thin Films of Bi_2Te_3 with Controlled Electronic Structure. *Adv. Mater.* **2011**, *23*, 2929–2932.
8. Linder, J.; Yokoyama, T.; Sudbø, A. Anomalous Finite Size Effects on Surface States in the Topological Insulator Bi_2Se_3. *Phys. Rev. B* **2009**, *80*, 205401.
9. Shan, W.-Y.; Lu, H.-Z.; Shen, S.-Q. Effective Continuous Model for Surface States and Thin Films of Three-Dimensional Topological Insulators. *New J. Phys.* **2010**, *12*, 043048.
10. Liu, C.-X.; Zhang, H. J.; Yan, B.; Qi, X.-L.; Frauenheim, T.; Dai, X.; Fang, Z.; Zhang, S.-C. Oscillatory Crossover

from Two-Dimensional to Three-Dimensional Topological Insulators. *Phys. Rev. B* **2010**, *81*, 041307(R).
11. Lu, H.-Z.; Shan, W.-Y.; Yao, W.; Niu, Q.; Shen, S.-Q. Massive Dirac Fermions and Spin Physics in an Ultrathin Film of Topological Insulator. *Phys. Rev. B* **2010**, *81*, 115407.
12. Chu, R.-L.; Shan, W.-Y.; Lu, J.; Shen, S.-Q. Surface and Edge States in Topological Semimetals. *Phys. Rev. B* **2011**, *83*, 075110.
13. Zhang, Y.; He, K.; Chang, C.-Z.; Song, C.-L.; Wang, L.-L.; Chen, X.; Jia, J.-F.; Fang, Z.; Dai, X.; Shan; *et al.* Crossover of the Three-Dimensional Topological Insulator Bi_2Se_3 to the Two-Dimensional Limit. *Nat. Phys.* **2010**, *6*, 584–588.
14. Sakamoto, Y.; Hirahara, T.; Miyazaki, H.; Kimura, S.-I.; Hasegawa, S. Spectroscopic Evidence of a Topological Quantum Phase Transition in Ultrathin Bi_2Se_3 Films. *Phys. Rev. B* **2010**, *81*, 165432.
15. Chang, C.-Z.; He, K.; Wang, L.-L.; Ma, X.-C.; Liu, M.-H.; Zhang, Z.-C.; Chen, X.; Wang, Y.-Y.; Xue, Q.-K. Growth of Quantum Well Films of Topological Insulator Bi_2Se_3 on Insulating Substrate. *SPIN* **2011**, *01*, 21–25.
16. Yazyev, O. V.; Moore, J. E.; Louie, S. G. Spin Polarization and Transport of Surface States in the Topological Insulators Bi_2Se_3 and Bi_2Te_3 from First Principles. *Phys. Rev. Lett.* **2010**, *105*, 266806.
17. Berntsen, M. H.; Goetberg, O.; Wojek, B. M.; Tjernberg, O. Direct Observation of Decoupled Dirac States at the Interface between Topological and Normal Insulators. *Phys. Rev. B* **2013**, *88*, 195132.
18. Liu, W.; Peng, X.; Wei, X.; Yang, H.; Stocks, G. M.; Zhong, J. Surface and Substrate Induced Effects on Thin Films of the Topological Insulators Bi_2Se_3 and Bi_2Te_3. *Phys. Rev. B* **2013**, *87*, 205315.
19. Zhang, G.; Qin, H.; Teng, J.; Guo, J.; Guo, Q.; Dai, X.; Fang, Z.; Wu, K. Quintuple-Layer Epitaxy of Thin Films of Topological Insulator Bi_2Se_3. *Appl. Phys. Lett.* **2009**, *95*, 053114.
20. Richardella, A.; Zhang, D. M.; Lee, J. S.; Koser, A.; Rench, D. W.; Yeats, A. L.; Buckley, B. B.; Awschalom, D. D.; Samarth, N. Coherent Heteroepitaxy of Bi_2Se_3 on GaAs (111)B. *Appl. Phys. Lett.* **2010**, *97*, 262104.
21. Tarakina, N. V.; Schreyeck, S.; Borzenko, T.; Schumacher, C.; Karczewski, G.; Brunner, K.; Gould, C.; Buhmann, H.; Molenkamp, L. W. Comparative Study of the Microstructure of Bi_2Se_3 Thin Films Grown on Si(111) and InP(111) Substrates. *Cryst. Growth Des.* **2012**, *12*, 1913–1918.
22. He, L.; Xiu, F.; Yu, X.; Teague, M.; Jiang, W.; Fan, Y.; Kou, X.; Lang, M.; Wang, Y.; Huang, G.; *et al.* Surface-Dominated Conduction in a 6 nm Thick Bi_2Se_3 Thin Film. *Nano Lett.* **2012**, *12*, 1486–1490.
23. Wang, Z. Y.; Guo, X.; Li, H. D.; Wong, T. L.; Wang, N.; Xie, M. H. Superlattices of Bi_2Se_3/In_2Se_3: Growth Characteristics and Structural Properties. *Appl. Phys. Lett.* **2011**, *99*, 023112.
24. Le, P. H.; Wu, K. H.; Luo, C. W.; Leu, J. Growth and Characterization of Topological Insulator Bi_2Se_3Thin Films on $SrTiO_3$ Using Pulsed Laser Deposition. *Thin Solid Films* **2013**, *534*, 659–665.
25. Schulz, H.; Thiemann, K. H. Crystal Structure Refinement of AlN and GaN. *Solid State Commun.* **1977**, *23*, 815–819.
26. Zhang, H.; Liu, C.-X.; Qi, X.-L.; Dai, X.; Fang, Z.; Zhang, S.-C. Topological Insulators in Bi_2Se_3, Bi_2Te_3 and Sb_2Te_3 with a Single Dirac Cone on the Surface. *Nat. Phys.* **2009**, *5*, 438–442.
27. Hytch, M. J.; Houdellier, F.; Hüe, F.; Snoeck, E. Nanoscale Holographic Interferometry for Strain Measurements in Electronic Devices. *Nature* **2008**, *453*, 1086–1089.
28. Nascimento, V. B.; Carvalho, V. E.; Paniago, R.; Soares, E. A.; Ladeira, L. O.; Pfannes, H. D. XPS and EELS Study of Bismuth Selenide. *Electron. Spectrosc. Relat. Phenom.* **1999**, *104*, 99–107.
29. Bansal, N.; Kim, Y. S.; Edrey, E.; Brahlek, M.; Horibe, Y.; Iida, K.; Tanimura, M.; Li, G.-H.; Feng, T.; Lee, H.-D.; *et al.* Epitaxial Growth of Topological Insulator Bi_2Se_3Film on Si(111) with Atomically Sharp Interface. *Thin Solid Films* **2011**, *520*, 224–229.
30. Kong, D.; Dang, W.; Cha, J. J.; Li, H.; Meister, S.; Peng, H.; Liu, Z.; Cui, Y. Few-Layer Nanoplates of Bi_2Se_3 and Bi_2Te_3 with Highly Tunable Chemical Potential. *Nano Lett.* **2010**, *10*, 2245–2250.
31. Bernandini, F.; Fiorentini, V.; Vanderbilt, D. Spontaneous Polarization and Piezoelectric Constants of III−V Nitrides. *Phys. Rev. B* **1997**, *56*, R10024.
32. Kinh, S. W.; Barnak, J. P.; Bremser, M. D.; Tracy, K. M.; Ronning, C.; Davis, R. F.; Nemanich, R. J. Cleaning of AlN and GaN Surfaces. *J. Appl. Phys.* **1998**, *84*, 5248.